Isochoric Heating of Solid Aluminum by Ultrashort Laser Pulses Focused on a Tamped Target

A. Saemann,[1] K. Eidmann,[1] I. E. Golovkin,[2] R. C. Mancini,[2] E. Andersson,[3] E. Förster,[3] and K. Witte[1]
[1]*Max-Planck-Institut für Quantenoptik, D-85748 Garching, Germany*
[2]*Department of Physics, University of Nevada, Reno, Nevada 89557-0058*
[3]*Institut für Optik und Quantenelektronik, Friedrich-Schiller-Universität, D-07743 Jena, Germany*
(Received 23 October 1998)

We have studied the K-shell emission of an Al plasma which was generated by focusing a high contrast 150 fs laser pulse at a wavelength of 395 nm and intensity of 5×10^{17} W/cm^2 on a flat Al target tamped by a thin surface layer of MgO. The measured resonance lines (Ly_α, He_α, and He_β) and their Li-like and He-like satellites are extremely broadened and show a red polarization shift. Analysis of the Ly_α and He_β satellites yields an electron temperature of $\approx$300 eV and an electron density of $(5-10) \times 10^{23}$ cm^{-3}. [S0031-9007(99)09405-3]

PACS numbers: 52.50.Jm, 52.25.Nr, 52.70.Kz

One fascinating aspect of the interaction of intense, ultrashort-duration laser pulses with matter is the possibility to generate plasmas at solid state density at high temperatures in the range 0.1 to 1 keV. Under these conditions the ion coupling parameter Γ [1] exceeds one and the plasma is thus in a strongly coupled state [2]. Such plasmas are of particular interest in inertial confinement fusion (ICF) and astrophysics. For example, it is possible to study the x-ray opacity of matter under conditions found in stellar interiors [3]. The importance for ICF originates from the fact that fs-laser generated plasmas approach temperatures and densities similar to the values currently attained in indirect drive experiments [4] and may therefore be of interest to investigate x-ray spectroscopy diagnostics needed for ICF plasmas [5]. In contrast to ICF plasmas, which require huge laser facilities, fs-laser plasmas can be generated by small tabletoplike lasers with a high repetition rate.

Here we report an experiment in which we focused a frequency doubled 150-fs Ti-Sapphire laser on tamped targets, which consisted of solid Al covered by a thin surface layer of MgO. We measured the Al K-shell emission by means of time-integrated high resolution crystal spectroscopy. The resonance and satellite lines were considerably broader than previously reported [6–9]. For the detailed spectral analysis, we used simultaneously the He-like satellites of the Ly_α line and the He_β line which is strongly merged with its Li-like satellites. To our knowledge these features have not been considered in previous studies of the x-ray emission from fs-laser plasmas. Our analysis indicates that we achieved a higher density compared to previous experiments where the electron density did not exceed a few times 10^{23} cm^{-3}. We attribute this result to the fact that we avoided early expansion by using a high contrast fs-laser pulse and tamped targets. Also the short wavelength of 395 nm may be helpful because it leads to absorption of the laser at a high critical density ($n_c = 7.2 \times 10^{21}$ cm^{-3}). Altogether, it was thus possible to produce ultrafast heating of solid Al before any significant expansion took place (i.e., isochoric heating).

The ATLAS Ti-Sapphire laser at the MPQ-Garching was used to produce pulses with 150 fs (FWHM), and 200 mJ at $\lambda = 790$ nm. To achieve a high contrast ratio, we frequency doubled the pulses and obtained 65–75 mJ at $\lambda = 395$ nm. The prepulse to main pulse contrast ratio has been measured at $\lambda = 790$ nm with an optical diode in the ns range and with a single shot second order autocorrelator in the ps range. From these measurements we expect after frequency doubling a contrast of 10^{-10} in the window 30 to 2 ns and of $\leq 10^{-6}$ at 1 ps before the peak of the pulse. By focusing with an off-axis parabola (f number = 2.7), we achieved a peak intensity of 5×10^{17} W/cm^2. A fraction of 75% of the laser energy is contained within a spot diameter of 20 μm with an average intensity of 10^{17} W/cm^2. This spot size corresponds to the region where the Al K-shell emission takes place, as measured by a penumbral technique [10]. Besides single laser pulses, we used double pulses consisting of two pulses of equal energy delayed by 25 ps to demonstrate the effect of a preformed plasma caused by a prepulse.

As targets, we used 9 mm thick diamond turned aluminum disks having a smoothly finished surface. In order to eliminate the rapid expansion of the Al front layers during the interaction with the laser pulse, we also used thin MgO layers acting as a tamper. The MgO layers were evaporated at a defined thickness on top of the aluminum disks. To make sure that the laser irradiates an undamaged target surface the target disks were mounted on a rotating target holder. All measurements were done under an angle of incidence of 30° with p-polarized light.

The K-shell emission of aluminum in the wavelength range 1.5–2.0 keV was measured with a von Hámos crystal spectrometer [11] equipped with a cylindrically bent pentaerythritol crystal with a lattice constant of $2d = 8.742$ Å. The direction of observation was along the normal to the target surface. The spectra were recorded on Kodak direct exposure film (DEF) [12]. We achieved

a resolving power $E/\Delta E$ better than 1500. With this setup it was possible to get a spectrum with 10–100 shots, depending on the intensity of the line under consideration.

Measured spectra are shown in Fig. 1 for three different cases. In Fig. 1a we utilized double pulses to generate a low density plasma for comparison with the high density spectra in Figs. 1b and 1c. These spectra were measured with high contrast single laser pulses using either plane aluminum disks (Fig. 1b) or aluminum disks tamped by a 300 Å thin layer of magnesium oxide evaporated on top of the aluminum (Fig. 1c).

Let us now compare the different spectra of Fig. 1. The typical low density Al spectrum of Fig. 1a shows a strong He_α line with the satellites of the different ions $Al^{5+\cdots10+}$ limited by the cold K_α line, furthermore, the He_β line with Li-like satellites and the Ly_α line. With a single pulse (Figs. 1b and 1c) all lines are much broader and the ratio of satellite to resonance line intensity is enhanced. The resonance lines ($He_{\alpha,\beta}$ and Ly_α) in the untamped Al target (Fig. 1b) have asymmetric profiles with a steeper wing on the high energy side. We attribute this to the fact that the plasma expands during the emission of the lines, which results in a lower density. Therefore the line profiles in Fig. 1b are caused by a superposition of the emission from a high and a low density plasma. This complicates a quantitative interpretation of the measured spectrum. In order to reduce spatial and temporal gradients, we used aluminum targets tamped by a 300 Å thick MgO layer. In Fig. 1c the effect of the tamper is demonstrated. The high energy wings of the He_α and Ly_α and, in particular, of the He_β are now flattened resulting in more symmetric line shapes and linewidths larger than those in Fig. 1b.

A surprising consequence of the tamper is the increase in Ly_α emission which may indicate a higher temperature in the tamped Al plasma. We have also recorded spectra with thicker MgO tamper layers. The Al emission decreases and finally vanished at tamper thicknesses between 1000 and 1500 Å. This indicates that the typical heated layer thickness is not larger than about 1500 Å. We will use this result below when we discuss opacity effects. It is noted that the MgO layers are considerably thicker than the skin depth, which is in the range 50–100 Å. Thus no laser light is expected to reach the Al.

An important finding is that we observe a redshift of the resonance lines ($He_{\alpha,\beta}$ and Ly_α) in the high density spectra in Figs. 1b and 1c. This is demonstrated by Fig. 2, which compares the Ly_α with its He-like satellites at low (double pulse) and high (single pulse) density. The Ly_α line at low density shows the fine structure due to the splitting of the upper level ($^2P_{1/2,3/2}$). In contrast, at high density the Ly_α is considerably broadened and clearly shifted. From Fig. 2 we find a center of gravity shift of 3.7 ± 0.7 eV. The shift can be determined with good accuracy because we simultaneously recorded in each spectrum the cold K_α line together with the other lines. Since the cold K_α line is neither shifted nor Stark broadened, it represents a good wavelength reference and allows us to accurately gauge the wavelength scale. The width of the K_α line is 1.4 eV (FWHM) (only slightly larger than the spectral resolution). Eventual small center

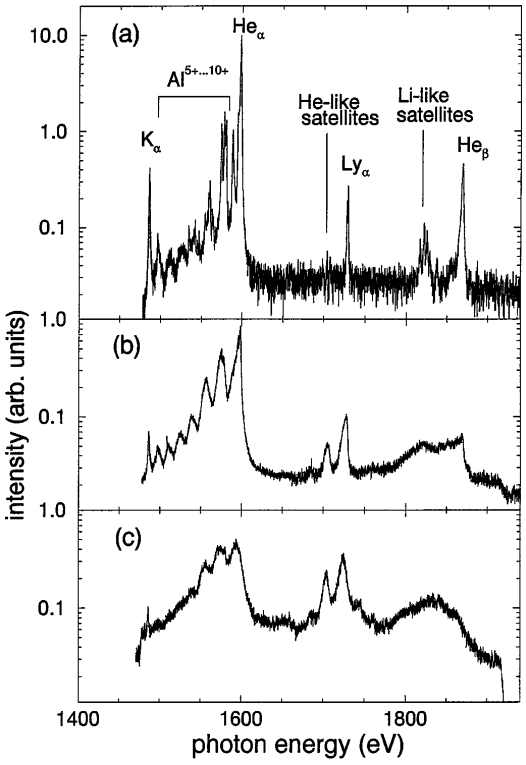

FIG. 1. Comparison between (a) measured low density plasma generated by double pulses, (b) mixture from low density and high density (see text), and (c) high density using an aluminum target tamped by a 300 Å thick MgO surface layer. The spectra are plotted in the same arbitrary units and therefore mutually comparable.

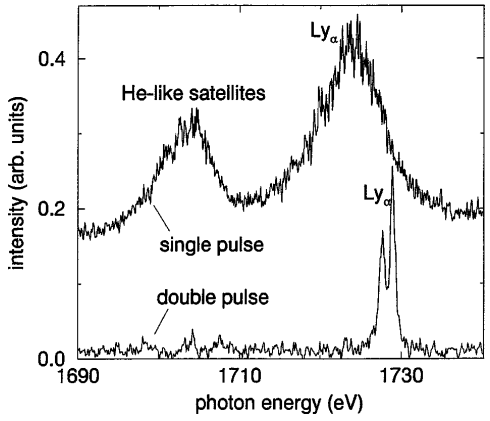

FIG. 2. Relative line shift of Ly_α between low density (double pulse, corresponding to Fig. 1a) and high density case (single pulse, corresponding to Fig. 1c). For clarity, the single pulse spectrum is shifted upward. The center of gravity shift of the Ly_α lines is 3.7 ± 0.7 eV.

of gravity shifts of the K_α due to contributions from $Al^{1+\cdots 4+}$ do not influence the result of Fig. 2 making the plausible assumption that the position of the K_α is the same for double and single pulses.

In addition to the time-integrated spectra, we also measured the duration of the overall Al K-shell emission by an ultrafast x-ray streak camera filtered by a thin foil with transmission above 1 keV. With a solid Al target irradiated by a single laser pulse (Fig. 1b) we find a duration of 2.5 ps (FWHM) [13]. Thus, most of the Al K-shell emission occurs after the laser irradiation.

The He_β and associated Li-like satellites, and the He-like satellites of the Ly_α line were analyzed using detailed line broadening, atomic kinetics, and radiation transport calculations. Stark-broadened line profiles were calculated using a multielectron radiator line profile code that takes into account the effects due to the microfields of the plasma ions and electrons [14,15]. Doppler broadening and the natural width of the lines are included, although at the high plasma densities considered here they make a small contribution. No line shifts were included in these line shape calculations. However, synthetic spectra were shifted in order to obtain the best overlapping with the experimental data.

To calculate the synthetic spectra, we solve self-consistently a set of steady-state collisional-radiative atomic kinetic rate equations and the radiation transport equation assuming a uniform slab geometry. The assumption of steady state may be justified by the high collisional rates of solid-density plasmas which bring the atomic kinetics close to a steady state during the (measured) emission duration of 2.5 ps. The physical thickness of the slab is 1400 Å, consistent with experimental arguments given above. Line overlapping between resonance and satellite transitions is important and dependent on the plasma conditions through the density sensitivity of the Stark-broadened line profiles. Radiation dependent rates are computed using Stark-broadened line shapes. Hence, the theoretical spectra has built-in temperature and density sensitivity through the level population distribution and the Stark-broadened line shapes.

For comparison with the experimental data, synthetic spectra were constructed using the radiation intensity distribution emerging along the normal to the plasma slab. Continuum background subtraction and instrumental broadening effects were also considered. Figure 3 shows the comparison between the experimental He_β and Li-like satellites' composite spectral feature and theoretical spectra calculated for electron densities and temperatures $n_e = 8 \times 10^{23}$ cm^{-3}, $T_e = 220$ eV and $n_e = 1 \times 10^{24}$ cm^{-3}, $T_e = 250$ eV. Since the experimental spectra are time and space integrated these densities and temperatures have to be interpreted as effective or average during the time of peak emission. The synthetic spectra include the He_β line in He-like Al as well as satellite transitions in Li-like Al with spectator electrons in $n = 2$, $n = 3$, and $n = 4$.

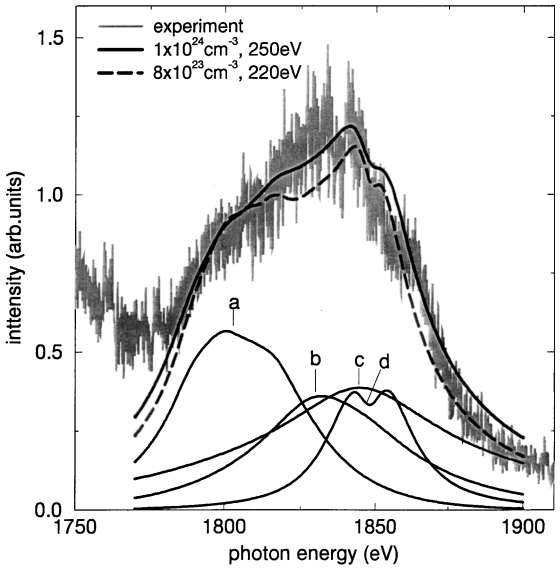

FIG. 3. Comparison of the He_β line and its satellites as measured with an aluminum target tamped by 300 Å MgO with calculations performed at different pairs of electron density and electron temperature as labeled in the figure. For one calculation ($n_e = 10^{24}$ cm^{-3} and $T_e = 250$ eV, thick solid line) also the individual overlapping contributions are shown, labeled as "a," "b," "c," and "d" for the transitions $1s2l3l'$-$1s^22l$, $1s3l3l'$-$1s^23l$, $1s3l4l'$-$1s^24l'$, and $1s3l$-$1s^2$, respectively.

For one calculated case ($n_e = 10^{24}$ cm^{-3} and $T_e = 250$ eV, thick solid curve), Fig. 3 shows the contributions of the individual line transitions labeled as "a," "b," "c," "d." At such high densities collisional excitation of the upper levels of satellite transitions is very effective and their intensities become comparable and even larger than that of the resonance line [16]. In turn, Stark broadening also increases for line transitions involving orbitals with high-n spectator electrons thus resulting in significant overlapping and blending. Hence, strong relative intensities and large line-broadening effects compete in determining the final shape of this composite spectral feature. For current conditions, the optical depth of this spectral feature is less than 0.25, and the difference between optically thick and thin calculations of the spectra is modest. Experiment-theory comparisons at lower densities underestimate the overall broadening and do not "fill" the gap in between He_β and $n = 2$ satellite lines, while calculations at larger densities overestimate the broadening.

While the He_α and Ly_α lines turn out to be optically thick and more subject to time- and space-integration problems, the $2l2l$-$1s2l$ He-like satellites of the Ly_α line present another interesting opportunity for spectroscopic analysis. Figure 4 shows theory-experiment comparisons for three combinations of n_e and T_e, with n_e in the range 5×10^{23} to 1×10^{24} cm^{-3} and T_e in the range 280 to 310 eV. We emphasize that, while the optical depth of the Ly_α can be larger than one, the optical depth of the $2l2l$-$1s2l$ satellites remains less than 0.2; this includes the effect of overlapping with the low-energy

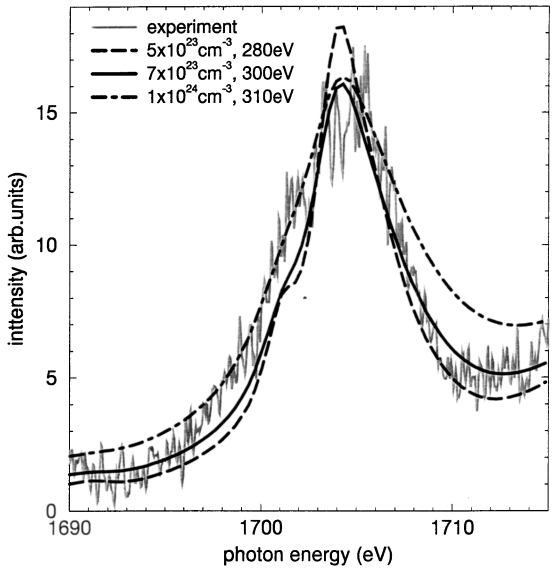

FIG. 4. Comparison of the He-like satellites of the Ly_α as measured with an aluminum target tamped by 300 Å MgO with calculations performed at different pairs of electron density and electron temperature as labeled in the figure.

wings of $2l3l$-$1s3l$ He-like satellite and $2p - 1s$ Ly_α transitions. Thus, opacity effects are small. While $n_e = 1 \times 10^{24}$ cm^{-3} overestimates the broadening and the slope of the high-energy wing, this spectral feature is indicative of plasma electron densities in the range 5×10^{23} to 7×10^{23} cm^{-3} thus showing good consistency with the high densities inferred from the analysis of the Li-like satellites and He_β spectral feature.

Thus, from the broadening of the Ly_α and He_β satellites we can infer an electron density close to the electron density of fully ionized solid aluminum which is 8×10^{23} cm^{-3}. A high density is also indicated by the large shift of the Ly_α line shown in Fig. 2. Calculation of the plasma polarization shift based on quantum-mechanical impact theory [17] yields for 8×10^{23} cm^{-3} and 300 eV a redshift of 3.5 eV which compares well with the measured value of 3.7 ± 0.7 eV, and with the shift used to fit the Ly_α satellites of 4 eV (see Fig. 4). All these lines involve $n = 2$ to $n = 1$ transitions. Furthermore, the shift of 20 eV deduced from the analysis of the He_β and Li-like satellites (3-1 transitions, see Fig. 3) also compares well with a theoretical estimate of 19 eV expected for the He_β line [18]. Hence, plasma conditions inferred from the spectroscopic analysis are consistent for the observed values of plasma polarization shifts. We note that these line shifts represent center-of-gravity shifts for the composite spectral feature. A complete analysis of the polarization shift of high density spectra is certainly an important issue for future line profile calculations. Note, for example, that the different transitions contributing to the overall satellite structure may be shifted by different amounts. Work is in progress to address these issues as well as details of the time history of the line spectra, and will be reported in a more extensive publication.

The high density at temperatures of a few 100 eV found in this experiment are also consistent with hydro calculations as will be discussed in detail elsewhere (compare also Ref. [19]). According to these calculations, the main mechanism for heating the dense target is the transport of the laser energy, absorbed in a thin front layer of the expanding tamper, into the solid Al by electron heat conduction. Also, at later times a shock wave develops competing with the electron heat wave. The compression caused by the shock wave could create densities exceeding solid density.

In conclusion, we have demonstrated isochoric heating of solid aluminum at temperatures around 300 eV. This corresponds to a pressure or energy density of $\approx$0.4 Gbar in the heated dense aluminum. The ion coupling parameter has a value of $\Gamma \approx 4$. Essential for achieving such a high density visible in the time-integrated K-shell spectra is that we avoided any early expansion of the Al target by using both a high contrast laser pulse and a tamped target. The dense plasma thus created is a convenient and reliable x-ray source constituting a test bed for spectroscopic studies under extreme conditions.

This work was supported in part by the commission of the European Communities in the framework of the Euratom-IPP association, the NSF Grant No. OSR-9353227, and the Max-Planck project under Contract No. 44188.

[1] S. Brush *et al.,* J. Chem. Phys. **45**, 2102 (1966).
[2] M. Nantel *et al.,* Phys. Rev. Lett. **80**, 4442 (1998).
[3] K. Nazir *et al.,* Appl. Phys. Lett. **69**, 3686 (1996).
[4] J. Lindl, Phys. Plasmas **2**, 3933 (1995).
[5] N. C. Woolsey *et al.,* Phys. Rev. E **57**, 4650 (1998).
[6] P. Audebert *et al.,* Europhys. Lett. **19**, 189 (1992).
[7] Z. Jiang *et al.,* Phys. Plasmas **2**, 1702 (1995).
[8] U. Teubner *et al.,* Appl. Phys. B **62**, 213 (1996).
[9] J. C. Gauthier *et al.,* Phys. Plasmas **4**, 1811 (1997).
[10] A. Saemann and K. Eidmann, Appl. Phys. Lett. **73**, 1334 (1998).
[11] L. v. Hámos, Ann. Phys. (Leipzig) **17**, 716 (1933).
[12] B. L. Henke *et al.,* J. Opt. Soc. Am. B **3**, 1540 (1986).
[13] K. Eidmann *et al.,* J. Quant. Spectrosc. Radiat. Transfer (to be published).
[14] L. A. Woltz and C. F. Hooper, Jr., Phys. Rev. A **38**, 4766 (1988).
[15] R. C. Mancini *et al.,* Comput. Phys. Commun. **63**, 314 (1991).
[16] R. C. Mancini *et al.,* Phys. Rev. E **54**, 4147 (1996).
[17] H. Nguyen *et al.,* Phys. Rev. A **33**, 1279 (1986).
[18] M. Koenig *et al.,* Phys. Rev. A **38**, 2089 (1988).
[19] G. Guethlein *et al.,* Phys. Rev. Lett. **77**, 1055 (1996).